JOURNAL OF COMPUTATIONAL PHYSICS 60, 534–548 (1985)

Solution of a Stefan Problem in the Theory of Laser Welding by the Method of Lines

MICHAEL DAVIS AND PHIROZE KAPADIA

Department of Physics, University of Essex, Colchester, United Kingdom

AND

JOHN DOWDEN

Department of Mathematics, University of Essex, Colchester, United Kingdom

Received March 2, 1984; revised November 6, 1984

Use of a laser beam as the source of energy for penetration welding gives rise to a long, thin cylindrical hole surrounded by molten metal. Material moves from the front to the rear of the hole as the workpiece is translated relative to the laser, by flowing around the hole. A computer program has been written which solves the equations governing a 2-dimensional steady-state mathematical model in which the only spatial variations considered are in a plane perpendicular to the axis of the hole. The program uses the method of lines applied to a reformulation of the problem suitable for solution by the isotherm migration technique. Computed results have been found to agree satisfactorily with those derived from an analytical model valid for low speeds of welding, and at higher speeds they give results similar to what is observed in practice, although lack of experimental evidence precludes a detailed quantitative comparison at present.

1. THE MATHEMATICAL MODEL

One of the many purposes for which lasers are used in industry is to supply the energy for welding; they are particularly well suited to penetration welding, where a laser beam is directed nearly perpendicularly to the workpiece, which is then moved in its own plane relative to the laser. A hole (usually referred to as a "keyhole") is created, and it is surrounded by molten metal. The weld forms as this liquid metal cools and solidifies downstream of the keyhole. A cross section of the keyhole perpendicular to the laser beam is shown in Fig. 1.

Mathematical models of the heat flow in penetration welding have been made by many authors [1, 2, 3] and analysis of this kind has been extended by Dowden, Davis, and Kapadia [4] to include a description of the flow of liquid metal around the keyhole from upstream to downstream of the laser beam. Approximate

0021-9991/85 $3.00

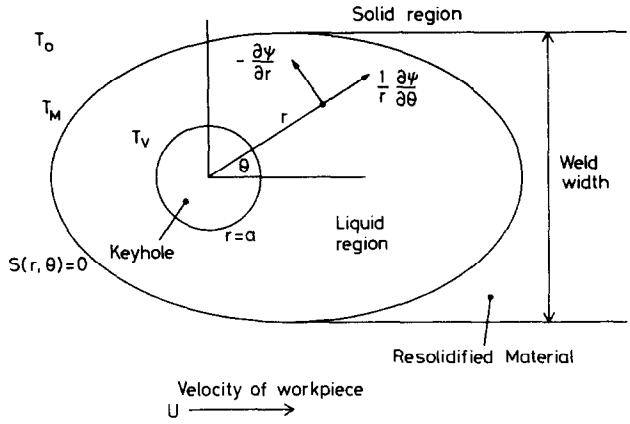

FIG. 1. Cross-section of the keyhole and molten region. The coordinate system employed is shown.

analytical solutions were presented, valid essentially for rather low speeds of translation of the workpiece. Four models were described which differed in the way in which the temperature dependence of the viscosity of the molten metal was taken into account. In qualitative terms there was in fact not a great deal of difference between the results for the more complicated assumptions when compared with the simplest assumption, that of a viscosity independent of temperature. It is the purpose of this paper to present a numerical program that solves this particular problem (with the assumption of a constant viscosity) over a range of speeds of translation U that includes all those used in practice. It was a weakness of the analytical solutions that they only just covered the lower end of this range.

The mathematical description employed here is the same as that of [4]. The mathematical parameters, including the viscosity μ are all assumed to be constants in each of the two regions, but the thermal conductivities k_S and k_L, as well as the thermal diffusivities κ_S and κ_L, of the solid and liquid regions respectively, are not necessarily taken to be the same. The density of the two regions, however, is taken to have the same value ρ for both states, in the interests of simplicity. Position in space is described by polar coordinates (r, θ) relative to axes moving with the laser beam, as shown in Fig. 1. Temperature in the metal is described by T with a vapourising temperature T_V, a melting temperature T_M, and a temperature T_0 far from the laser; the latent heat of fusion is L. Velocity is described by means of a stream function ψ so that the radial velocity is $\partial\psi/r\partial\theta$ and the azimuthal velocity is $-\partial\psi/\partial r$. Only a steady-state solution in these axes is sought.

With this description the complete set of equations and conditions are as follows [4]: In the solid region the temperature distribution is governed by the differential equation

$$\frac{1}{r}\left\{\frac{\partial T}{\partial r}\frac{\partial\psi}{\partial\theta}-\frac{\partial T}{\partial\theta}\frac{\partial\psi}{\partial r}\right\}=\kappa_S\nabla^2 T, \tag{1}$$

while in the liquid region the temperature equation is

$$\frac{1}{r}\left\{\frac{\partial T}{\partial r}\frac{\partial \psi}{\partial \theta}-\frac{\partial T}{\partial \theta}\frac{\partial \psi}{\partial r}\right\}=\kappa_L \nabla^2 T \tag{2}$$

and the Navier–Stokes equations for the fluid velocity of the liquid metal can be reduced to the 2-dimensional vorticity equation

$$\frac{\rho}{r}\left\{\frac{\partial \nabla^2 \psi}{\partial r}\frac{\partial \psi}{\partial \theta}-\frac{\partial \nabla^2 \psi}{\partial \theta}\frac{\partial \psi}{\partial r}\right\}=\mu \nabla^4 \psi. \tag{3}$$

The boundary conditions are

$$\left.\begin{aligned} \psi &= 0 \\ T &= T_V \\ \frac{\partial \psi}{\partial r} &= r\frac{\partial^2 \psi}{\partial r^2} \end{aligned}\right\} \quad \text{at } r=a, \tag{4}$$

$$\left.\begin{aligned} \psi &= Ur\sin\theta \\ \frac{\partial \psi}{\partial r} &= U\sin\theta \\ [k\nabla T]^{\text{Solid}}_{\text{Liquid}}\cdot \nabla S+\frac{L\rho}{r}\cdot\frac{\partial(S,\psi)}{\partial(r,\theta)} &= 0 \\ T &\to T_0 \qquad \text{as } r\to\infty. \end{aligned}\right\} \quad \text{at } S(r,\theta)=0, \tag{5}$$

In conditions (5), $S(r, \theta)=0$ is the equation of the interface between the solid and liquid regions. Solutions are sought for which T is an even function of θ, and ψ is odd. These two symmetries can be used to reduce the amount of computer memory required in the calculation of the solution.

Equations (1) and (2) for the temperature distribution and Eq. (3) for the stream function have to be solved subject to the boundary conditions (4). These are statements of the requirement that the sides of the keyhole should be a stream surface at the temperature of vapourisation of liquid metal, on which no tangential stress is being exerted. The assumption of an isothermal surface suggests that there will be no surface tension gradients from thermal causes. It is just possible that surface active elements might produce them in the way that can happen on the surface of the weld pool in conventional welding [5], but the possibility is ignored here. A small amount of material in fact is vapourised at the keyhole surface; it can be ignored for the purposes of calculating the motion of the molten metal, but is important for the physics of the keyhole. Its vapourisation provides an ablation pressure [6] whose variation round the surface of the keyhole drives the motion of the liquid metal. The first two parts of condition (5) require both components of

velocity to be continuous across the solid/liquid interface, and the third part is the heat-flow condition. In the solid region T tends to a constant value as $r \to \infty$ and the stream function ψ is everywhere $Ur \sin \theta$.

2. Method of Solution

The technique known as the method of lines (or semidiscretisation) was used to solve (1)–(3). It is essentially a technique for replacing a system of partial differential equations in two or more independent variables by an approximate system of ordinary differential equations in one of these variables. Other methods such as finite differences, finite element, or implicit methods seemed either unsuitable or impractical for solving this particular set of partial differential equations with their boundary conditions; with these methods the main difficulty arises in handling the moving boundary at the solid/liquid interface, as the program code which results tends to be very expensive on CPU time.

The method of lines has a number of advantages over the other algorithms, namely that it can be used to solve every type of partial differential equation, whether elliptic, parabolic, or hyperbolic, as well as ordinary differential equations other than those of eigenvalue type. The overall implementation on a computer is relatively easy and it is not expensive on CPU time or memory for a given run. There is, however, one drawback, which is that the domain of the independent variables must be a topological rectangle. This disadvantage can usually be avoided by a transformation of the coordinate system; currently, attempts are being made to overcome the problem of arbitrarily shaped boundaries and to develop dynamic automatic line spacing algorithms for non-linear problems with moving wavefronts to gain runtime efficiency.

In one space dimension, the Stefan problem can be illustrated by means of the following differential equations

$$\begin{aligned} \rho C_1 \frac{\partial T_1}{\partial t} &= \frac{\partial}{\partial x} k_1 \frac{\partial T_1}{\partial x}, \qquad 0 < x < S(t), \\ \rho C_2 \frac{\partial T_2}{\partial t} &= \frac{\partial}{\partial x} k_2 \frac{\partial T_2}{\partial x}, \qquad x > S(t). \end{aligned} \tag{6}$$

The conditions at the interface as $x \to S(t)$ are

$$\begin{aligned} T_1 &= T_2 = T_M \\ k_2 \frac{\partial T_2}{\partial x} - k_1 \frac{\partial T_1}{\partial x} &= -\rho L \frac{dS}{dt}, \end{aligned} \tag{7}$$

where k is the thermal conductivity, ρ is the density, C the heat capacity, L the latent heat, and T the temperature. The subscript (1) refers to the solid region and

(2) to the liquid region. There are also the boundary conditions $T = T_0$ at $x = 0$ and $T \to T_\infty$ as $x \to \infty$ as well as an initial condition at $t = 0$. It is then necessary to find $T_1(x, t)$, $T_2(x, t)$, and $S(t)$.

There is no difficulty in writing down and solving suitable finite difference equations, with intervals Δx and Δt, in the main parts of the liquid and solid regions. The problem arises near the interface, partly due to the discontinuity in the temperature gradient, and partly because the coordinate of a new mesh point on the line $t + \Delta t$ is not known; consequently it is not known in which region the points P and Q in Fig. 2 are located. This information is implicit in the differential equations and the interface conditions. Usually some iterative process is required to obtain a solution of the non-linear system. The resulting finite difference equation must be reasonably accurate (i.e., the local truncation error should be small), and also the system must be stable, so that as Δt and $\Delta x \to 0$ the computed solution tends to the correct solution. In practice the resulting finite difference equations are very complex in nature [7, 8]. As an alternative, Meyer [9] has used a scheme in which the t variable is discretised, and which with the weak solution method has been applied to a number of problems [10, 11]. The approach used here however is the isotherm migration technique. In this method the dependent and the independent variables are exchanged. In the Stefan problem a solution for T is sought which is expressed as a function of x and t, or by changing the independent variable the problem is converted into one in which x is sought as a function of T and t. Since (7) shows that the moving boundary (as well as the other two) is an isotherm, it becomes a fixed straight line in the new co-ordinate system parallel to the t axis, and the free boundary condition appears as a condition at one of the boundaries. The isotherm migration technique is particularly suitable for extensions

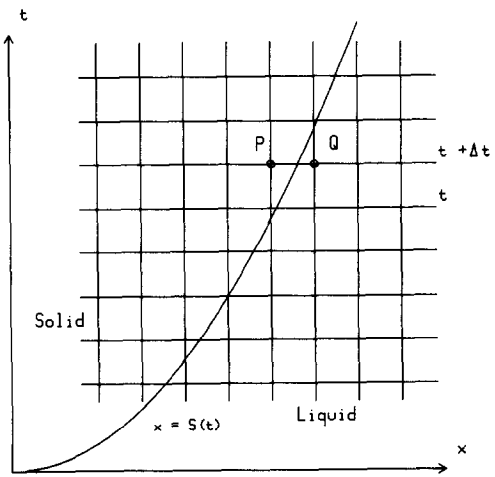

FIG. 2. Relationship between the unknown boundary $x = S(t)$ and the grid points used in calculation.

of this work to take account of the temperature dependence of most of the material parameters; most of them depend on T, which in this formulation is one of the independent variables of the computation, not one of the dependent variables.

Equations (6) with conditions (7) transformed in this way become

$$\rho C_1 \frac{\partial x_1}{\partial T} = -\frac{\partial}{\partial T}\left(k_1 \Big/ \frac{\partial x_1}{\partial T}\right), \qquad T_0 < T < T_M,$$

$$\rho C_2 \frac{\partial x_2}{\partial T} = -\frac{\partial}{\partial T}\left(k_2 \Big/ \frac{\partial x_2}{\partial T}\right), \qquad T_M < T < T_\infty,$$

$$x_1 = 0 \qquad \text{when } T = T_0,$$

$$x_2 \to \infty \qquad \text{as } T \to T_\infty,$$

$$\left[k \Big/ \frac{\partial x}{\partial T}\right]_1^2 = -\rho L \frac{\partial x}{\partial t} \qquad \text{on } T = T_M,$$

$$[x]_1^2 = 0 \qquad \text{at } T = T_M.$$

Crank and Phahle [12] used a finite difference method to solve a slightly simpler version of this problem and the only difficulty with the technique is that a small Δt is required for stability as the resulting equations are nonlinear.

Weak solution, finite element, and variational methods have all been used to solve Stefan problems. The technique used here however is the method of lines, with Lagrangian differentiation formulae. The resulting set of differential equations are then solved using the latest developments in initial value algorithms.

Equations (1)–(3) and the associated boundary conditions can now be transformed into the new coordinate system (T, θ) so that the problem is described in a rectangular domain. The moving boundary at the interface is fixed in these coordinates and the condition on it becomes a condition at this known, fixed boundary. The change of variables from (r, θ) to (T, θ) coordinates is lengthy, but can be performed with the aid of the differential relations

$$\frac{\partial T}{\partial r} = 1 \Big/ \frac{\partial r}{\partial T}, \qquad \frac{\partial T}{\partial \theta} = -\frac{\partial r}{\partial \theta} \Big/ \frac{\partial r}{\partial T},$$

$$\frac{\partial f(r, \theta)}{\partial r} = \frac{\partial T}{\partial r} \frac{\partial f(T, \theta)}{\partial T},$$

$$\frac{\partial f(r, \theta)}{\partial \theta} = \left\{\frac{\partial T}{\partial \theta} \frac{\partial}{\partial T} + \frac{\partial}{\partial \theta}\right\} f(T, \theta).$$

So, for example,

$$\frac{\partial f}{\partial r}\frac{\partial \psi}{\partial \theta} - \frac{\partial f}{\partial \theta}\frac{\partial \psi}{\partial r} = \left\{\frac{\partial f}{\partial T}\frac{\partial \psi}{\partial \theta} - \frac{\partial f}{\partial \theta}\frac{\partial \psi}{\partial T}\right\} \Big/ \frac{\partial r}{\partial T}$$

and

$$\frac{\partial^2 T}{\partial r^2} = -\frac{\partial^2 r}{\partial T^2} \Big/ \left(\frac{\partial r}{\partial T}\right)^3.$$

The transformation requires that $\partial T/\partial r \neq 0$; experience with the analytical solution, as well as physical expectation, suggests that this will be so. Problems far from the keyhole were avoided by giving σ a large but finite value when $T = T_0$. In practice, no difficulties attributable to these causes were experienced in the computation.

With r and ψ as the unknown functions and subscripts T and θ used to indicate partial differention, the equation are as follows: (1) becomes

$$\kappa_S \left\{ -\frac{r r_{TT}}{r_T^2} + 1 + \frac{2 r_\theta r_{\theta T}}{r r_T} - \frac{r_\theta^2 r_{TT}}{r r_T^2} - \frac{r_{\theta\theta}}{r} \right\} - U(r_\theta \sin\theta + r\cos\theta) = 0; \tag{8}$$

(2) can be written

$$\kappa_L \left\{ -\frac{r r_{TT}}{r_T^2} + 1 + \frac{2 r_\theta r_{\theta T}}{r r_T} - \frac{r_\theta^2 r_{TT}}{r r_T^2} - \frac{r_{\theta\theta}}{r} \right\} - \psi_\theta = 0; \tag{9}$$

with $\omega = -\nabla^2 \psi$, (3) is

$$\omega = -\frac{\psi_{TT}}{r_T^2}\left(1 + \frac{r_\theta^2}{r^2}\right) + \frac{2\psi_{T\theta} r_\theta}{r^2 r_T} - \frac{\psi_{\theta\theta}}{r^2} + \frac{\psi_T}{r_T} \times \left\{ \frac{r_{TT}}{r_T^2}\left(1 + \frac{r_\theta^2}{r^2}\right) + \frac{r_{\theta\theta}}{r^2} - \frac{2 r_{T\theta} r_\theta}{r^2 r_T} - \frac{1}{r} \right\}, \tag{10}$$

provided that ω satisfies

$$\mu \nabla^2 \omega = \frac{\rho}{r}\left\{ \frac{\partial \omega}{\partial r}\frac{\partial \psi}{\partial \theta} - \frac{\partial \omega}{\partial \theta}\frac{\partial \psi}{\partial r} \right\},$$

i.e.,

$$\omega_\theta \psi_T r r_T + \frac{\mu}{\rho}\{\omega_{TT}(r^2 + r_\theta^2) - 2\omega_{T\theta} r_\theta r_T + \omega_{\theta\theta} r_T^2\} + \left(\kappa_L - \frac{\mu}{\rho}\right)\frac{\omega_T}{r_T}\{r_{TT}(r^2 + r_\theta^2) + r_{\theta\theta} r_T^2 - 2 r_{\theta T} r_\theta r_T - r r_T^2\} = 0. \tag{11}$$

These have to be solved in $|\theta| \leqslant \pi$, $T_0 < T < T_V$ as shown in Fig. 3. The boundary conditions in this new coordinate system are

$r \to \infty$ as $T \to T_0$

r is continuous across $T = T_M$

$\psi/r = [\psi_T/r_T]^{\text{Solid}}_{\text{Liquid}} = U \sin\theta$ at $T = T_M$

$[k/r_T]^{\text{Solid}}_{\text{Liquid}} + rUL\rho(r_\theta \sin\theta + r\cos\theta)/(r^2 + r_\theta^2) = 0$ at $T = T_M$.

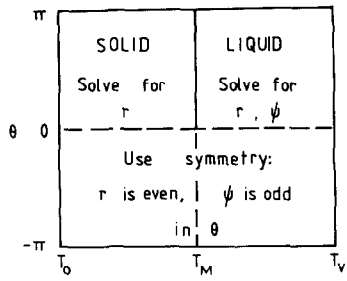

FIG. 3. The domain of computation.

The third of these conditions expresses the requirement that both components of the velocity vector must be continuous, while the last is the equivalent of (5). The conditions at the keyhole are that, at $T = T_V$,

$$r = a$$

$$\psi = 0$$

$$\psi_{TT} - \psi_T r_{TT} = r_T^2 \psi_T / a.$$

The last of these is the equivalent of (4); with the aid of (10) and the previous two conditions it can be put in the simpler form

$$\omega = -2\psi_T / a r_T.$$

The use of the shooting method in connection with the method of lines, presents the problem of constructing a suitable strategy which will ensure convergence to the correct solution for a large system of ordinary differential equations. Accordingly, to solve the above elliptic problem by the method of lines without resorting to shooting methods, artifical time derivatives are added to the above equations to convert them into parabolic form. They are then integrated from an initial condition (an estimate of $r(T, \theta)$ and $\psi(T, \theta)$) until the time derivatives approach zero; the left-hand sides of (8) and (9) are therefore equated to $\partial r/\partial t$ and the left-hand side of (11) to $\partial\omega/\partial t$. If the signs in front of the time derivatives were changed the numerical solution would diverge; Lagrangian differentiation formulae could not be used to approximate the derivatives, as errors would be generated during the numerical integration.

The equations in the solid and liquid regions were generated by two subroutines written in FORTRAN. In the solid region they were approximated by 20 points in the T direction and 20 points in the θ direction, producing a system of 400 ordinary differential equations. The liquid region differed slightly in that 10 points were used in the T direction and 20 points in the θ direction. This produces a system of 2×200 ordinary differential equations, and the factor of 2 arises because there are two equations: the Navier–Stokes equation and the heat conduction equation describing the liquid region.

The boundary conditions are handled by the stagewise differentiation method (Schiesser [13]) and the time derivatives at the boundary points are zeroed before the subroutines are returned back to the calling program. This is to control error waves starting at the boundary points and is discussed further below. In effect the boundary points are evaluated algebraically rather than by numerical integration.

Before the method of lines can be started an estimate of the moving boundary is obtained. A steady-state solution is then generated for both the liquid and solid regions. Equipped with this solution the moving boundary is then tested to see if a preassigned error criterion is satisfied. If it is not, the moving boundary is adjusted by a Newton-type iteration scheme of the form

$$S(r, \theta_i) \text{ is replaced by } S(r, \theta_i) + \tau\varepsilon(1 + |S(r, \theta_i)|) \quad \text{for } i = 1, 2, \ldots, 20,$$

where $S(r, \theta_i)$ is the boundary function, τ the magnitude of the boundary shift, and the error ε is given by

$$\varepsilon = \left[\frac{C_p \kappa}{r_T}\right]_{\text{Liquid}}^{\text{Solid}} + \frac{rUL(r_\theta \sin\theta + r\cos\theta)}{r^2 + r_\theta^2}.$$

The procedure is repeated until the error criterion is satisfied.

The equations generated by the method of lines were integrated by one of the following integrators.

(i) Gear–Hindmarsh algorithm [14, 15], i.e., the Gear backward differentiation formulae for stiff equations. The Jacobian matrix is assumed to be banded and is calculated by finite differences, and interpolation is performed to reach the end of the print interval.

(ii) The same as (i), but no interpolation is performed to reach the end of the print interval.

(iii) Gear–Hindmarsh algorithm, with the Jacobian matrix replaced by a diagonal approximation based on a directional derivative. Interpolation is performed to reach the end of the print interval.

(iv) The same as (iii), but no interpolation is performed to reach the end of the print interval.

(v) Runge-Kutta–Fehlberg algorithm.

Since the equations that occur in the mathematical modelling of the laser welding process are highly stiff, the Runge-Kutta–Fehlberg method is expensive on computer time compared to the Gear algorithm. It has nevertheless been included to enable a comparison of results to be effected using two different integrator methods, and thus serve as a mutual check on each other.

The accuracy of the method of lines algorithm is governed by the number of spatial divisions, the order of the spatial coupling and the truncation error of the integration algorithm. The first two dominate the overall error control in the

method, and the integration algorithms adjust the integration step so that the local truncation error of each variable is below a specified maximum. This error is the local error at each integration step, and these errors can accumulate over a number of steps to cause a large global error. However in a stable algorithm these errors tend to cancel rather than accumulate, so the global error does not grow at an unacceptable rate. The latter also depends on the equation-set being solved.

An increase in the number of spatial divisions increases the accuracy but it also increases the stiffness of the resulting set of ordinary diffeential equations, thus causing a lower maximum integration step size. Increasing the spatial coupling increases the accuracy, but also increases the CPU time required to evaluate higher order formulae. Five-point formulae were used to solve the modified form of Eqs. (8) and (11) and this represented the optimum trade-off between accuracy and CPU time. The overall error in this implementation of the method of lines is approximately given by $1/N^2$, where N is the number of grid points defining the discretisation.

In the discretisation of the independent variables using a constant order formula, the errors increase by several orders of magnitude from central to border points. This is an effect which has been minimised by using higher order formulae at points near the boundaries, but there will be a finite nonzero limit to the process of convergence to the steady state. The values computed for the artificial time derivative thus merely represent the closest attainable approach to zero.

3. Implementation of the Laser Welding Model in FORTRAN

The laser welding problem as described by the analytical models of [4] and the numerical procedure described here were all incorporated in a single program, written to a standard of FORTRAN 10 [16].

In the numerical model "infinity" is initially assumed to be located at a distance of 10 cm from the keyhole and is adjusted, if necessary, to obtain stability. If the welding velocity U is very slow, the initial guess for the moving boundary is obtained from the analytical solution. The tolerance prescribed for the numerical

TABLE I

The Performance Figures of the Five Integrators Contained in the Program, Using a DEC System 10

Integration option	CPU time	Number of iterations
(i)	7 min 18.8 s	2
(ii)	15 min 43.6 s	2
(iii)	6 min 28.6 s	2
(iv)	11 min 50.0 s	2
(v)	40 min 57.7 s	2

Note. Details of options (i)–(v) are in the text.

TABLE II

Values of the Physical Parameters Employed in Calculations for Four Different Metals[a]

		Iron	Titanium	Aluminium	Lead
T_V	(°C)	2726	3287	2467	1740
T_M	(°C)	1371	1675	658.7	327.4
ρ	(g cm^{-3})	7.2	4.45	2.7	11.34
L	(J g^{-1})	266.7	418.7	397.8	23.03
μ	(g cm^{-1} s^{-1})	0.0225	0.0225[b]	0.0105	0.017
k_s	(J cm^{-1} s^{-1} °C^{-1})	0.694	0.2	2.37	0.346
κ_s	(cm^2 s^{-1})	0.213	0.0859	0.975	0.235
k_L	(J cm^{-1} s^{-1} °C^{-1})	0.327	0.1[b]	1.03	0.0637
κ_L	(cm^2 s^{-1})	0.0551	0.028[b]	0.351	0.0407

[a] In all cases the ambient temperature T_0 was taken as 20°C.
[b] Values employed in the absence of detailed measurements.

integrator is 5.0×10^{-5}. The error prescribed for the moving boundary is 0.01 and the relative shift for the moving boundary is 0.001. The performance figures of the integrators are shown in Table I using the values for the physical constants listed in the first column of Table II.

A typical calculation was performed with $U = 0.75$ cm s^{-1} and $a = 0.019$ cm. The value for a is somewhat small for industrial applications, but was chosen for purposes of comparison with samples provided by the Welding Institute (Cambridge, U.K.). The program works equally satisfactorily for larger values. The numbers given in the first column of Table II are those appropriate to the material of the sample, a mild steel.

The stream function for the liquid region is shown in Fig. 4 as a 3-dimensional plot together with its contour map in Fig. 5. Likewise 3-dimensional plots for the temperature in the solid and liquid regions are given, to different scales, in Figs. 6 and 7, respectively; a contour map for both regions in the vicinity of the keyhole is given in Fig. 8. Results for the same value of U, but with a very slightly smaller keyhole size ($a = 0.015$ cm) were obtained for the approximate analytical solution

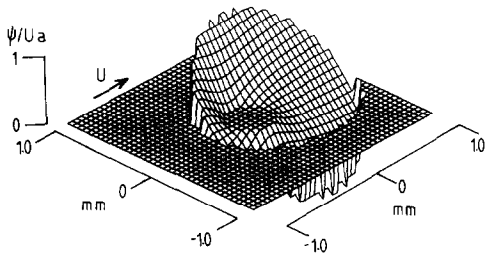

FIG. 4. Graph of the stream function in the liquid region for iron with $U = 0.75$ cm s^{-1} and $a = 0.19$ mm.

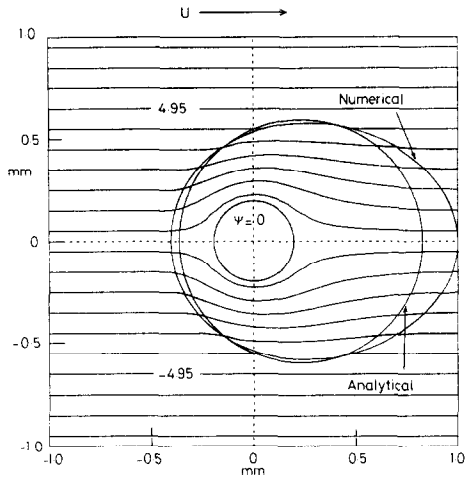

FIG. 5. Streamlines for the same solution; contours are at intervals of 0.761 $mm^2 s^{-1}$.

and were reported in [4]. A comparison of the figures shown there with the ones presented here reveals how closely the two solutions agree. The shape of the liquid region as predicted by the analytical solution is superimposed on Fig. 5, and it can be seen that they are very close. The greatest difference is that the numerical model predicts a shape which extends further downstream, as would be expected in practice.

For comparison purposes, and to enable an assessment to be made of the effect of variation of material parameters, numerical solutions were also obtained for titanium, aluminium, and lead, for which values of the constants are also shown in Table II. Aluminium was chosen as it is the main element in many alloys which are welded by lasers in industry. The choice of titanium was determined by the fact that it is known to be a very difficult material to weld by conventional means (e.g., TIG welding), but is easily welded with a laser. It is a metal that is used widely in high technology areas together with stainless steel. Additionally, as a material it has a

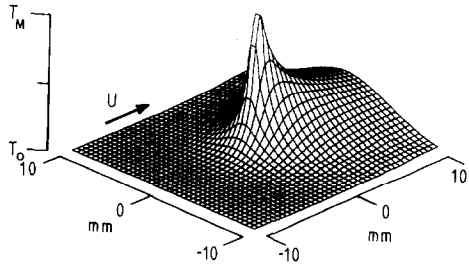

FIG. 6. Graph of the temperature distribution in the solid region

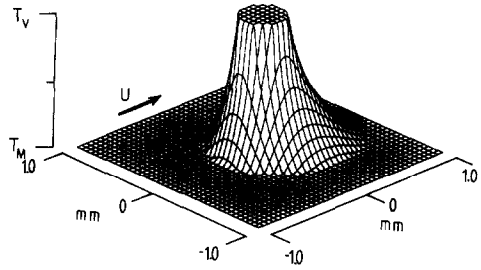

FIG. 7. Graph of the temperature distribution in the liquid region.

very high melting and vapourisation temperature, as well as a high value for the latent heat compared with iron. The choice of lead as another material for numerical study was suggested by a desire to secure the largest extreme practical variation in material parameters possible, as compared with titanium, although it is not in fact a practical material for use in laser welding. The constants in question for lead are at the opposite extreme from titanium: namely, lead has a very low latent heat of fusion as well as a low vapourisation temperature.

In the analytical model, when the weld velocity U is strictly zero, Laplace's equation for the temperature has an ($\ln r$)-type singularity in two dimensions which causes a pile-up of heat flux, thus prohibiting the physical realisation of a steady-state solution. The numerical program is therefore arranged to terminate for a value of U less than 0.01 cm s^{-1}. For values of U somewhat greater than this but still within the range of validity of the theoretical model, the results obtained by the program agreed well with the approximate results obtained by the analytical model.

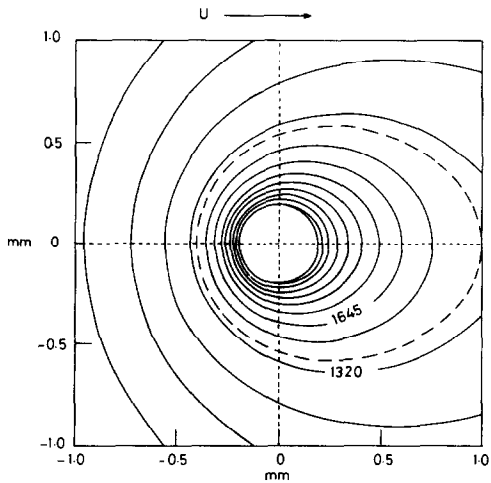

FIG. 8. Isotherms in the liquid and solid regions. Contours are at intervals of 162.5°C and the broken line shows the position of the boundary between two regions.

The value of the numerical program lies in the fact that it can deal with weld speeds for which the analytical model ceases to be valid. There is an upper limit of $U = 20\ \text{cm}\ s^{-1}$ set by a combination of the method used and overflow in floating point arithmetic in the machine. This weld speed, however, more than adequately covers the range used in practice, which extends from about 0.75, to 5 cm s^{-1}.

The variation in material constants can best be seen when one fixes the size of the keyhole and the weld speed and displays the appropriate moving boundaries for several different materials on a single diagram. Figure 9 shows them for titanium, iron, aluminium, and lead; note the progressively increasing size of the molten pool around the keyhole as one considers these materials in turn. It will be seen that lead has a considerably more elongated molten region than the other metals, and it is possible that this is due to the fact that its melting temperature is much lower relative to its vapourising temperature than is the case for the others.

Another physical parameter of interest is the power used, and this can be obtained by integrating the gradient of the temperature field numerically in the liquid region. Table III displays the values of the power for iron over a range of weld speeds and includes a comparison with the values for the power provided by the analytical model. In all cases the keyhole size is given by $a = 0.01$ cm.

In conclusion it remains to note that the models of laser welding presented here agree with the experimental welding process in all its general features. In the absence of detailed knowledge of all the physical parameters (including their dependence on temperature) it is not at present possible to secure a more exact comparison with the limited range of experimental measurements available. The 2-dimensional models presented here and in [4] are the first to consider the motion of the liquid phase in detail and to display the moving boundary in question. The good agreement of the numerical model in the range of parameters for which both

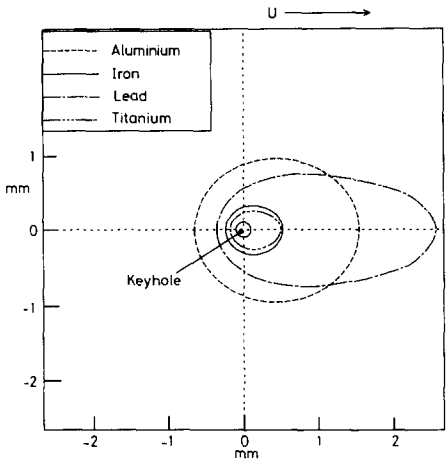

FIG. 9. Shape of the boundaries between the solid and liquid regions for four different metals. In all cases $U = 1\ \text{cm}\ \text{s}^{-1}$ and $a = 0.1$ mm.

TABLE III

Power and Weld Width for Various Values of the Weld Speed, Calculated for Iron and Compared with the Values Given by the Approximate Analytical Model [4]; $a = 0.01$ cm

Velocity ($cm\ s^{-1}$)	Power ($W\ cm^{-1}$)		Weld width (cm)	
	Computed	Analytical model	Computed	Analytical model
0.1	1389	1406	0.1472	0.1450
0.5	1915	1902	0.0810	0.0865
0.75	2132	2087	0.0718	0.0759
1.0	2318	2243	0.0662	0.0693
2.0	2925	2732	0.0545	0.0554
3.5	3662	3317	0.0467	0.0463
5.0	4314	3840	0.0425	0.0413

are valid is an encouraging check on the analysis underlying the program and on its implementation; the inclusion of the liquid phase is an essential step in the direction of experimental reality. The availability of a program capable of calculating the heat and fluid flow at a range of welding speeds of practical significance opens up the way to further experimental and theoretical work.

REFERENCES

1. D. T. SWIFT-HOOK AND A. E. F. GICK, *Welding J. (Miami)*, **52** (1973), 492_s.
2. P. G. KLEMENS, *J. Appl. Phys.* **47** (1976), 2165.
3. W. W. DULEY, "CO_2 Lasers: Effects and Applications," Chap. 4., Academic Press, New York/London, 1976.
4. J. M. DOWDEN, M. DAVIS, AND P. KAPADIA, *J. Fluid Mech.* **126** (1983), 123.
5. C. R. HEIPLE AND J. R. ROPER, *Welding J. (Miami)*, **61** (1982), 97_s.
6. J. G. ANDREWS AND D. R. ATTHEY, *J. Phys. D* **9** (1976), 2181.
7. J. DOUGLAS AND T. M. GALLIE *Duke Math. J.* **22** (1955), 557.
8. L. FOX, *in* "Moving Boundary Problems in Heat Flow and Diffusion" (J. R. Ockendon and W. R. Hodgkins, Eds.), Oxford Univ. Press (Clarendon), London/New York, 1975.
9. G. H. MEYER, *Numer. Math.* **16** (1970), 248.
10. G. H. MEYER, *J. Inst. Math. Applic.* **20** (1977), 317.
11. G. H. MEYER, *Numer. Math.* **29** (1978), 329.
12. J. CRANK AND R. D. PHAHLE, *Bull. Inst. Math. Applic.* **9** (1973), 12.
13. W. E. SCHIESSER, "DSS/2: An Introduction to the Numerical Method of Lines Integration of Partial Differential Equations," Lehigh University, Bethlehem, Pa., 1977.
14. C. W. GEAR, "Numerical Initial Value Problems in Ordinary Differential Equations," Prentice–Hall, Englewood Cliffs, N. J., 1971.
15. A. C. HINDMARSH, "GEARB: Solution of Ordinary Differential Equations Having Banded Jacobian," UCRL-30059, Lawrence Livermore Laboratory, Livermore, Calif., 1973.
16. Digital Equipment Corporation, "DEC System 10: FORTRAN Programmer's Reference Manual," Maynard, Mass, 1982.